




REGULAR PAPER

Effect of oxygen shielding on the tensile and fatigue performance of 300M repaired through laser-directed energy deposition

C. Barr^{1,4}, R.A.R. Rashid^{2,4}, S. Palanisamy^{2,4}, N. Matthews^{3,4} and M. Brandt^{1,4}

¹RMIT Centre for Additive Manufacturing, Carlton, VIC, Australia, ²School of Engineering, Faculty of Science, Engineering and Technology, Swinburne University of Technology, Melbourne, VIC, Australia, ³Rosebank Engineering, Bayswater, VIC, Australia and ⁴DMTC Ltd, Hawthorn, VIC, Australia

Corresponding author: C. Barr; Email: cameron.barr@rmit.edu.au

Received: 28 April 2023; Revised: 25 September 2023; Accepted: 28 September 2023

Keywords: Repair; additive manufacturing; steels; tensile properties; fatigue

Abstract

Laser-directed energy deposition (L-DED) is a key enabling technology for the repair of high-value aerospace components, as damaged regions can be removed and replaced with additively deposited material. While L-DED repair improves strength and fatigue performance compared to conventional subtractive techniques, mechanical performance can be limited by process-related defects. To assess the role of oxygen on defect formation, local and chamber-based shielding methods were applied in the repair of 300M high strength steel. Oxidation between layers for locally shielded specimens is confirmed to cause large gas pores which have deleterious effects on fatigue life. Such pores are eliminated for chamber shielded specimens, resulting in an increased ductility of ~15%, compared to ~11% with chamber shielding. Despite this, unmelted powder defects are not affected by oxygen content and are found in both chamber- and locally shielded samples, which still have negative consequences for fatigue.

Nomenclature

AM	additive manufacturing
HAZ	heat-affected zone
L-DED	laser-directed energy deposition
R	fatigue loading ratio (minimum load/maximum load)
SEM	scanning electron microscopy
300M/300M	L-DED deposited 300M steel onto 300M substrate
Δt	cooling time between deposited layers

1.0 Introduction

Additive manufacturing (AM) continues to gain significant attention in the aerospace industry, as maturing technologies allow for the creation of new lightweight designs with enhanced functionality [1]. This not only extends to new aircraft, but also to existing ones, with AM technologies providing a major avenue for lowering sustainment costs by reducing the need for spare parts, increasing aircraft readiness and improving the flexibility of supply chains [2]. One area for enhanced sustainability is the refurbishment of damaged components through laser directed energy deposition (L-DED) [1, 3]. This

A version of this paper first appeared at The Australian International Aerospace Congress 2021 (AIAC19).

process uses a laser beam to locally melt a target substrate and build up additional material by delivering pneumatically blown powder to the melt-pool. In repair, damaged regions of existing component are machined out and then replaced by the deposited material. This is highly advantageous compared to traditional subtractive repair, as the restoration of load bearing area allows for structural repairs to be carried out, while also being compatible with modern component design where little excess material is available for removal.

The high cost of aerospace components, long lead times in production, and significant financial and operational losses associated with grounded aircraft makes aerospace a key market for additive repair. Indeed, a comprehensive review of over 440 articles found aviation to be the largest industrial sector for the deployment of the additive repair, making up 35% of sector specific publications [3]. Major success has been found in the repair of worn turbine blades and blisks [4–6], with excellent performance from titanium [7] and nickel-based superalloys [8]. Unique adaptations to L-DED further allow for the repair of single crystal blades without inducing new grain orientations [9, 10]. The repair of ultra-high strength steels for landing gear applications have also attracted much interest, with repairs conducted using 4,340 [11], 420SS [12], Aermet100 [13, 14], and 300M [15, 16]. Repair of 300M is of particular concern for several reasons. Firstly, the extreme tensile strength of 2,000MPa comes at the cost of fracture toughness, which places the steel at great risk of crack propagation from fatigue and impact with foreign objects during take-off and landing. Second, 300M is highly prone to corrosion if left unprotected, as it lacks the additional alloying elements used in modern stainless steels. Finally, as few steels can match the strength of 300M, it is one of the primary steels used in landing gear and thus presents a high volume of potentially damaged parts.

Given the low fracture toughness of 300M, ensuring the L-DED process does not induce additional defects is of great concern. Poorly optimised deposits can be prone to cracking, lack of fusion defects and inter-run porosity between tracks and layers [17], while other defects such as gas pores and unmelted powders can persist even with optimised parameters. Both gas pores and unmelted powders were found to be the primary initiator of fatigue failure in repaired 300M coupons [16], particularly when located close to the surface. Unmelted powders can be trapped when plunging into the melt-pool and caught by the rapidly advancing solidification front. The finer gas pores may have several origins, either caused by powder interactions with the melt-pool [18], entrained porosity in the feed powders [18], vaporisation due to excessive laser power [19] or the evolution of dissolved gasses [19]. A third, much larger type of gas pore was also identified in the above study, which were suggested to be caused by the build-up of oxides between layers due to the limited gas shielding supplied by the deposition nozzle. This follows the results of two different steel powders with different oxygen contents, with high oxygen (5,300ppm) resulting in significant porosity and limited mechanical performance, while the low oxygen case (280ppm) showed no porosity and good performance [20].

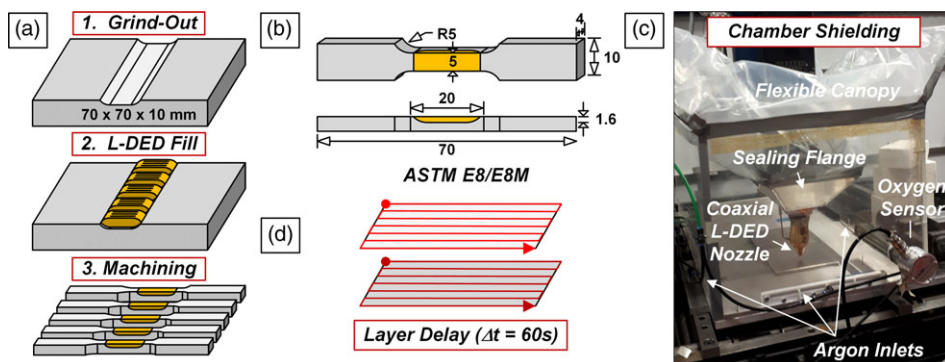
Given the major negative effects of the large gas pores on tensile [20] and fatigue behaviour [16], this study seeks to confirm the role of oxygen on their formation and its influence on other defects. To eliminate potential oxidation between deposited layers, this study utilises chamber-based argon shielding to purge environmental oxygen from the deposition process. The chamber shielded samples will be compared to the locally shielded equivalent and the subsequent differences in tensile and fatigue performance explored.

2.0 Materials and methods

300M is a martensitic ultra-high strength steel with very little alloy content. Quench and tempered plates of 300M with dimensions of $70 \times 70 \times 20$ mm were prepared for tensile specimens, with gas atomised metal 300M powder with a size range of 50–100 μ m sieved for the feed material. Two different powder batches were used during testing, as long-term powder storage may lead to oxygen contamination over time. Existing quantities of 300M supplied by Sandvik Ltd was used for locally shielded specimens, while a new batch of 300M powder supplied by Carpenter Technology was used for the chamber shielded specimens. The chemical compositions of the substrate and metal powders are shown in Table 1.

Table 1. 300M substrate composition and feed powder compositions for the local and chamber shielding specimens

300M	Fe	C	Cr	Mn	Mo	Ni	Si	V
Substrate	Bal.	0.43	0.82	0.83	0.39	1.88	1.64	0.07
Local	Bal.	0.30	0.91	0.78	0.39	1.90	1.60	0.08
Chamber	Bal.	0.42	0.80	0.81	0.40	1.77	1.60	0.08

**Figure 1.** Overview of the L-DED repair testing, showing (a) summary of the repair process, (b) tensile sample dimensions, (c) scan path for deposition and (d) argon chamber setup.

The L-DED repair process is shown in Fig. 1(a), while the intended tensile specimen dimensions are shown in Fig. 1(b). Substrates were slotted along the centre to a depth of 1.8mm with a blend radius of 6mm and sandblasted ready for deposition. L-DED was conducted on a TRUMPF TruLaser Cell 7020 system using a 3.0kW disk laser ($\lambda = 1,030\text{nm}$) and coaxial laser cladding head with motorised optics for spot size control. The spot size was set at 1.3mm, with deposited tracks spaced by 0.65mm (i.e. 50% overlap). Deposition was carried out using 800W laser power, a scan rate of 1,050mm/min. Powder was delivered at 4.6g/min using a helium gas at a flow rate of 10L/min. Localised nozzle shielding was provided using argon gas at a flow rate of 16L/min. A specially constructed enclosure was also used to provide chamber shielding to select samples (Fig. 1(c)), which was initially purged of oxygen to below 10ppm and maintained using an argon flow rate of 10L/min and supplemented by the 16L/min nozzle gas.

Deposition was restricted only to where the mechanical specimens were to be machined, with a raster pattern used to deposit an area of $25 \times 10\text{mm}$. A 60 second delay between layers was used to facilitate the in-situ tempering of the 300M deposit (as shown in Fig. 1(d)) [15], as bulk heat treatment of repaired components should be avoided. Deposition was continued until at least three layers were present above the original surface. These layers were machined away, along with the top 0.2mm of the surface to ensure that 40% of the cross-section contained deposited material, and that all untempered martensite in the top layers was removed.

Tensile specimens were prepared in accordance with ASTM E8/E8M with testing performed on a 250kN MTS machine equipped with a laser extensometer, using a strain rate of 10^{-3} s^{-1} . Tested specimens were sectioned perpendicular to the loading direction to observe the microstructure behind the fracture surface, with the specimens polished to a $1\mu\text{m}$ finish before being etched with a 3% Nital solution for metallographic examination. Macrostructures and fracture surfaces were observed using optical microscopy (Olympus BX-61) and scanning electron microscopy (SEM, Phillips XL30).

3.0 Results and discussion

Oxygen shielding is necessary to avoid largescale defects in L-DED processed steels, with the macrostructure of a non-shielded specimen shown in Fig. 2(a), where severe porosity is present. Both

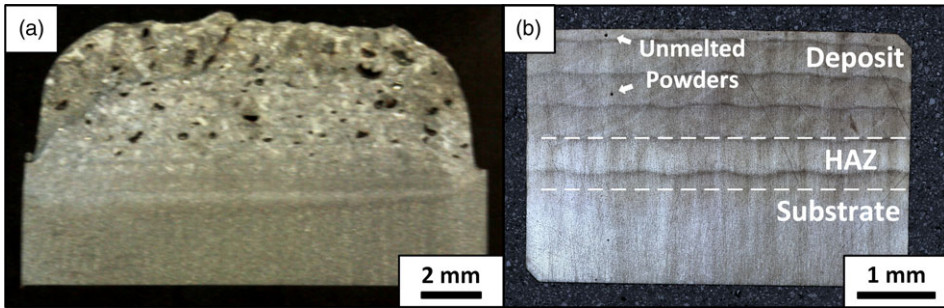


Figure 2. Effect of shielding on sample macrostructure, with (a) the cross-section of an un-shielded 300M deposit, and (b) repaired 300M/300M with local shielding, which shows the same features as chamber shielding.

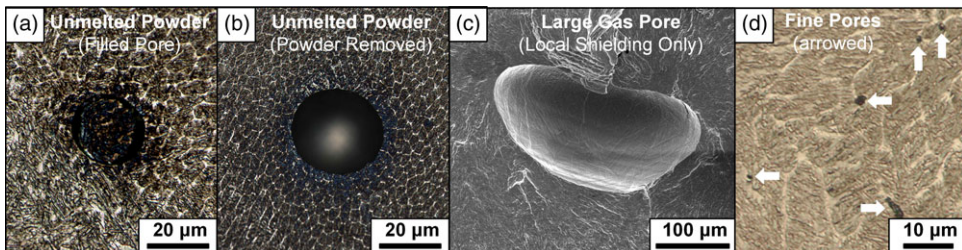


Figure 3. Common defects in the repaired samples including, (a) filled and (b) unfilled pores related to unmelted powders, (c) very large gas pores found in the fracture surfaces of a locally shielded fatigue samples [16] and (d) very fine pores found with both shielding types.

locally shielded and chamber shielded specimens are effective at eliminating such defects, with the two strategies producing macrostructures similar to Fig. 2(b). The alternating bands of dark and light etching correlate to successive cycles of in-situ tempering with each layer, with darker etching corresponding to tempering at higher temperature, thereby exhibiting lower hardness [15]. The similarity in tempering is related to the shared thermal history between the two deposition strategies. The difference in shielding environment is unlikely to have a major impact in this regard, as heat conduction through the large substrate block is likely to account for the majority of heat dissipation, particularly with the layer delay. The groove geometry also limits the area available to convection, further reducing the impact of environment type.

While deposition was optimised, some isolated defects remained as shown in Fig. 3. Unmelted powders were a common defect for both shielding types with sizes up to $50\mu\text{m}$. These were found in either a partially fused state (Fig. 3(a)) or as spherical pores if removed during cross-sectioning (Fig. 3(b)). This occurs when powders plunge into the melt-pool and rapidly solidify when encountering the edges of the melt-pool. Given local shielding protects the region directly below the coaxial nozzle, it is difficult for chamber shielding to provide further protection against this type of defect. Very large gas pores up to $300\mu\text{m}$ in length are only found in locally shielded samples at the interface between tracks and layers (Fig. 3(c)), similar to the pores in the unshielded specimen. Combined with the purple discolouration with local shielding, such pores are a likely result of oxidation, as they were not present with chamber shielding. The formation of large pores is also likely to be a rare event compared to unmelted powders, as they were only revealed on the fracture surfaces of tested specimens. Despite this, their appearance in the fracture surfaces suggest they can have a significant deleterious effect on mechanical behaviour. Finally, very fine pores ($<1\mu\text{m}$) were also found with both shielding types, but do not appear to have a

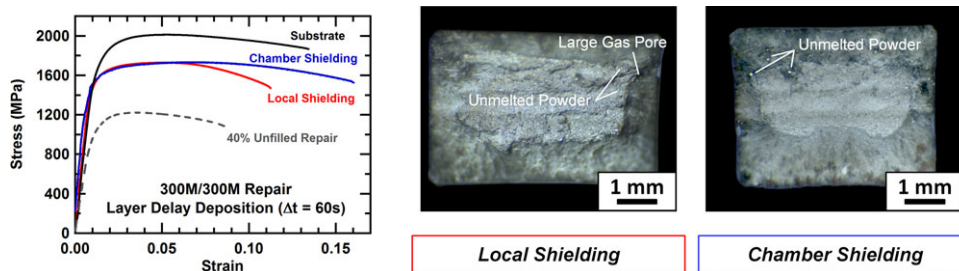


Figure 4. Tensile results for 300M/300M samples, showing stress strain behaviour and corresponding fracture surfaces.

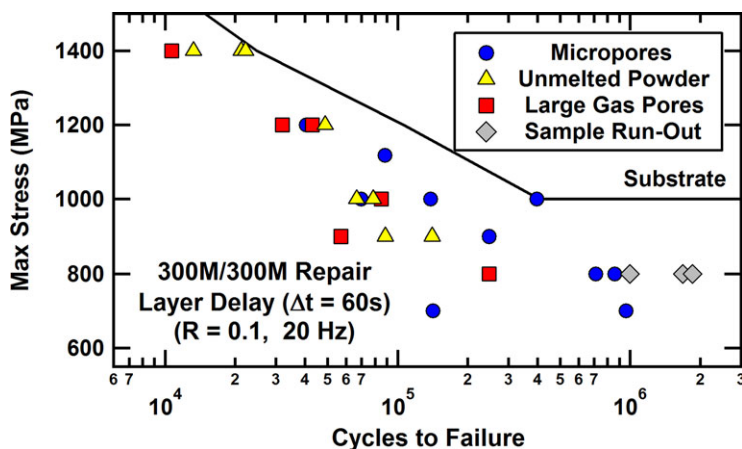


Figure 5. Influence of defects on the fatigue performance for locally shielded 300M/300M repairs [16], with the worst performance linked to large gas pores that are eliminated with chamber shielding. Unmelted powder defects are still problematic for chamber shielding.

distinct cause. Such pores may be related to the entrapment of gasses during deposition regardless of shielding type [18], with bubbles unable to escape to the surface due to strong Marangoni flow in the melt pool [21].

The tensile results are shown in Fig. 4(a), with both shielding types exhibiting the same strength but with increased ductility in the chamber shielded specimen. Studies on AM 300M reveal that different deposition parameters, scan paths and AM technologies can lead to variations in tensile properties [16, 22]. This is due to differences in peak temperature during deposition, resulting in samples with higher heat inputs over-softening during in-situ tempering and exhibiting lower strength. As discussed above, the thermal history is expected to be near identical for both shielding types, which should lead to similar strength. The only difference between the shielding types is ductility, which in turn is strongly influenced by the type and number of defects present in the samples. The corresponding fracture surfaces in Fig. 4(b)–(c) show both samples displaying ductile fracture with well-developed shear lips. While unmelted powder defects are revealed for both surfaces, the locally shielded specimens are known to contain large gas pores, which may suggest other oxide related defects. Such defects may be sufficient to initiate earlier fracture compared to the unmelted powder defects, which were present in both samples. Reduced ductility through defects is a common theme for AM materials, with their elimination seen as a key means for improving performance [23]. While further work is underway to examine how the different compositions affect tensile behaviour, it is possible that the high temperature softening of 300M

is more significant than the strength imparted by additional carbon above 0.30 wt.%, again leading to similar strength.

The presence of defects has larger implications for fatigue performance in AM materials, which have shown to be the key initiator of failure in locally shielded 300M repairs [16]. Figure 5 shows a summary of the different defect types on fatigue life for local shielding. As seen, large gas pores have the most detrimental effect on fatigue life, followed closely by unmelted powder defects. Although chamber shielding can eliminate the large pores, the continued presence of unmelted powders remains problematic for chamber shielding, with alternative strategies required for their removal. Further investigation is underway to characterise the effect of chamber shielding on fatigue performance, as the enhanced ductility of the tensile specimens suggests that fatigue behaviour may also be improved.

4.0 Conclusions

Chamber shielding is shown to be an effective method for improving the ductility of L-DED repaired 300M, though strength remains the same as the locally shielded samples. The equivalent strength for both shielding strategies is related to similar thermal histories experienced during deposition, which act to heat treat the deposit without need for further processing. Large gas pores are found in locally shielded specimens are confirmed to be related to oxidation, as they can be eliminated via chamber shielding leading to improved ductility. Despite this, fine pores and unmelted powder defects remain, which require further optimisation of the L-DED process to eliminate. This is important for fatigue applications, as unmelted powder defects show similar deleterious effects on fatigue life as the large gas pores from oxidation.

Acknowledgements. This paper includes research that was supported by DMTC Limited (Australia). The authors have prepared this paper in accordance with the intellectual property rights granted to partners from the original DMTC project. The authors acknowledge the use of facilities within the RMIT Advanced Manufacturing Precinct, as well as the RMIT Microscopy and Microanalysis Facility for its support and thank the staff for their support.

References

- [1] Liu, R., Wang, Z., Sparks, T., Liou, F. and Newkirk, J. 13 - Aerospace applications of laser additive manufacturing, in *Laser Additive Manufacturing*, Brandt, M., Ed, Woodhead Publishing, 2017, pp 351–371.
- [2] Kundu, S., Jones, R., Peng, D., Matthews, N., Alankar, A., Raman, S.R. and Huang, P. Review of requirements for the durability and damage tolerance certification of additively manufactured aircraft structural parts and AM repairs, *Materials*, 2020, **13**, (6), p 1341.
- [3] Kanishka, K. and Acherjee, B. A systematic review of additive manufacturing-based remanufacturing techniques for component repair and restoration, *J. Manuf. Processes*, 2023, **89**, pp 220–283.
- [4] Nowotny, S., Scharek, S., Beyer, E. and Richter, K.-H. Laser beam build-up welding: precision in repair, surface cladding, and direct 3D metal deposition, *J. Therm. Spray Technol.*, 2007, **16**, pp 344–348.
- [5] Kelbassa, I., Gasser, A. and Wissenbach, K. Laser cladding as a repair technique for BLISKS out of titanium and nickel base alloys used in aero engines, Pacific International Conference on Applications of Lasers and Optics, Laser Institute of America, 2004.
- [6] Richter, K.-H., Orban, S. and Nowotny, S. Laser cladding of the titanium alloy Ti6242 to restore damaged blades, Proceedings of the 23rd International Congress on Applications of Lasers and Electro-optics, 2004.
- [7] Choi, Y.R., Sun, S.D., Liu, Q., Brandt, M. and Qian, M. Influence of deposition strategy on the microstructure and fatigue properties of laser metal deposited Ti-6Al-4V powder on Ti-6Al-4V substrate, *Int. J. Fatigue*, 2020, **130**, p 105236.
- [8] Chaurasia, J.K., Jinoop, A., Paul, C., Bindra, K., Balla, V.K. and Bontha, S. Effect of deposition strategy and post processing on microstructure and mechanical properties of serviced Inconel 625 parts repaired using laser directed energy deposition, *Opt. Laser Technol.*, 2024, **168**, p 109831.
- [9] Chen, H., Lu, Y., Luo, D., Lai, J. and Liu, D. Epitaxial laser deposition of single crystal Ni-based superalloys: Repair of complex geometry, *J. Mater. Process. Technol.*, 2020, **285**, p 116782.
- [10] Liu, Z. and Qi, H. Effects of processing parameters on crystal growth and microstructure formation in laser powder deposition of single-crystal superalloy, *J. Mater. Process. Technol.*, 2015, **216**, pp 19–27.
- [11] Da Sun, S., Liu, Q., Brandt, M., Luzin, V., Cottam, R., Janardhana, M. and Clark, G. Effect of laser clad repair on the fatigue behaviour of ultra-high strength AISI 4340 steel, *Mater. Sci. Eng. A*, 2014, **606**, pp 46–57.

- [12] Da Sun, S., Fabijanic, D., Barr, C., Liu, Q., Walker, K., Matthews, N., Orchowski, N., Easton, M. and Brandt, M. In-situ quench and tempering for microstructure control and enhanced mechanical properties of laser clad AISI 420 stainless steel powder on 300M steel substrates, *Surface Coat. Technol.*, 2018, **333**, pp 210–219.
- [13] Lourenço, J.M., Da Sun, S., Sharp, K., Luzin, V., Klein, A.N., Wang, C.H. and Brandt, M. Fatigue and fracture behavior of laser clad repair of AerMet[®] 100 ultra-high strength steel, *Int. J. Fatigue*, 2016, **85**, pp 18–30.
- [14] Walker, K., Lourenço, J., Sun, S., Brandt, M. and Wang, C. Quantitative fractography and modelling of fatigue crack propagation in high strength AerMet[®] 100 steel repaired with a laser cladding process, *Int. J. Fatigue*, 2017, **94**, pp 288–301.
- [15] Barr, C., Da Sun, S., Easton, M., Orchowski, N., Matthews, N. and Brandt, M. Influence of delay strategies and residual heat on in-situ tempering in the laser metal deposition of 300M high strength steel, *Surface Coat. Technol.*, 2020, **383**, p 125279.
- [16] Barr, C., Rashid, R.A.R., Da Sun, S., Easton, M., Palanisamy, S., Orchowski, N., Matthews, N., Walker, K. and Brandt, M. Role of deposition strategy and fill depth on the tensile and fatigue performance of 300M repaired through laser directed energy deposition, *Int. J. Fatigue*, 2021, **146**, p 106135.
- [17] Zhong, C., Gasser, A., Schopphoven, T. and Poprawe, R. Experimental study of porosity reduction in high deposition-rate Laser Material Deposition, *Opt. Laser Technol.*, 2015, **75**, pp 87–92.
- [18] Ahsan, M.N., Bradley, R. and Pinkerton, A.J. Microcomputed tomography analysis of intralayer porosity generation in laser direct metal deposition and its causes, *J. Laser Appl.*, 2011, **23**, (2), p 022009.
- [19] Svetlizky, D., Zheng, B., Buta, T., Zhou, Y., Golan, O., Breiman, U., Haj-Ali, R., Schoenung, J.M., Lavernia, E.J. and Eliaz, N. Directed energy deposition of Al 5xxx alloy using Laser Engineered Net Shaping (LENS[®]), *Mater. Des.*, 2020, **192**, p 108763.
- [20] Dong, Z., Kang, H., Xie, Y., Chi, C. and Peng, X. Effect of powder oxygen content on microstructure and mechanical properties of a laser additively-manufactured 12CrNi2 alloy steel, *Mater. Lett.*, 2019, **236**, pp 214–217.
- [21] Chouhan, A., Aggarwal, A. and Kumar, A. A computational study of porosity formation mechanism, flow characteristics and solidification microstructure in the L-DED process, *Appl. Phys. A*, 2020, **126**, (11), pp 1–12.
- [22] Jing, G., Huang, W., Yang, H. and Wang, Z. Microstructural evolution and mechanical properties of 300M steel produced by low and high power selective laser melting, *J. Mater. Sci. Technol.*, 2020, **48**, pp 44–56.
- [23] Sanaei, N. and Fatemi, A. Defects in additive manufactured metals and their effect on fatigue performance: a state-of-the-art review, *Prog. Mater. Sci.*, 2020, p 100724.